

# Finite-temperature Gutzwiller approximation and the phase diagram of a toy-model for $V_2O_3$

Matteo Sandri,<sup>1</sup> Massimo Capone,<sup>1</sup> and Michele Fabrizio<sup>1</sup>

<sup>1</sup>*International School for Advanced Studies (SISSA),  
and CNR-IOM Democritos, Via Bonomea 265, I-34136 Trieste, Italy*

(Dated: February 21, 2013)

We exploit exact inequalities that refer to the entropy of a distribution to derive a simple variational principle at finite temperature for trial density matrices of Gutzwiller and Jastrow type. We use the result to extend at finite temperature the Gutzwiller approximation, which we apply to study a two-orbital model that we believe captures some essential features of  $V_2O_3$ . We indeed find that the phase diagram of the model bears many similarities to that of real vanadium sesquioxide. In addition, we show that in a Bethe lattice, where the finite temperature Gutzwiller approximation provides a rigorous upper bound of the actual free energy, the results compare well with the exact phase diagram obtained by the dynamical mean field theory.

PACS numbers: 71.10.-w, 71.10.Fd, 71.30.+h

## I. INTRODUCTION

A genuine Mott insulator, where the insulating character is due exclusively to charge localization, is a very useful concept, physically conceivable, but never realized in the ground state of known correlated materials. Indeed, no system can sustain at zero temperature the residual entropy that would be associated with all other electronic degrees of freedom different from charge. As a result, Mott localization is always accompanied at low temperature by other phenomena that freeze those degrees of freedom, for instance magnetic ordering or structural distortions, which effectively turn the Mott insulator into a conventional band insulator. By this we mean the possibility of reproducing low-temperature static and often also dynamic properties of a supposed Mott insulator by an independent-particle scheme, no matter how sophisticated it is.<sup>1</sup> However, even though it provides satisfactory results, an independent-particle scheme, like Hartree-Fock or DFT within LDA and its extensions, has a drawback: it can describe only the simultaneous locking of charge and other degrees of freedom, like spin or lattice, while in a Mott insulator the charge freezes at a much higher energy scale than any other degree of freedom.

A tool that can reveal this hierarchy of energy scales typical of a Mott insulator is the temperature, which unveils the profound difference between the excited states of a Mott insulator and those of its “band-insulator” counterpart<sup>2</sup>.

The typical example are antiferromagnetic Mott insulators, e.g.  $La_2CuO_4$  or Cr-doped  $V_2O_3$ , whose conducting properties remain insulating-like also above the Néel temperature, while any independent particle scheme would predict metallic behavior as soon as Néel order melts. It is therefore important to have at disposal theoretical tools able to deal with strong correlations and finite temperature. One that is currently adopted is dynamical mean field theory (DMFT)<sup>3</sup> in combina-

tion with local-density approximation (LDA)<sup>4</sup> or the GW approximation<sup>5</sup>. These combined methods are extremely reliable for correlated materials, but they can become extremely cumbersome and numerically demanding, especially if full consistency on the density is required.

More recently, there have been several attempts to combine efficiently and self-consistently LDA with the Gutzwiller variational approach within the Gutzwiller approximation (GA),<sup>6-8</sup> which is less accurate but much simpler and less demanding than DMFT. So far, these attempts have been restricted to ground state properties, hence to zero temperature. A finite temperature extension of the GA has actually been proposed in Ref. 9, but only in the simplest case of the one-band Hubbard model, where it was shown to reproduce qualitatively well the exact DMFT phase diagram.<sup>9</sup> However, in order to tackle more realistic models, it would be desirable to have at disposal a finite temperature generalization of the GA able to deal with generic multi-band models.

This is actually the aim of the present work that is organized as follows. First, in section II we derive a rigorous upper-bound estimate of the free-energy of a many-body Hamiltonian within the class of Gutzwiller- and Jastrow-like variational density matrices. Next, in section III we specialize to the case of Gutzwiller-like density matrices and introduce the Gutzwiller approximation at finite temperature. In section IV, we introduce a simple model for vanadium sesquioxide,  $V_2O_3$ , show how to implement in practice the Gutzwiller approximation at finite temperature, section IV A, and discuss its results at zero and finite temperature, , section IV B and IV C, respectively. In section V we compare the phase diagram obtained by the Gutzwiller approximation on a Bethe lattice with the exact one obtained by DMFT. Finally, section VI is devoted to concluding remarks.

## II. VARIATIONAL ESTIMATE OF THE FREE ENERGY

In this section we shall repeatedly use some known trace inequalities, for which we refer the reader to Ref. 10. Let us consider an interacting many-body system described by the interacting Hamiltonian  $\mathcal{H}$  at finite temperature  $T > 0$ . It is known that the free-energy functional

$$F(X) = \text{Tr}(X\mathcal{H}) + T \text{Tr}(X \ln X), \quad (1)$$

with the matrix  $X > 0$  and such that  $\text{Tr} X = 1$ , is minimized by the Boltzmann distribution function

$$X_{\min} = \frac{e^{-\beta\mathcal{H}}}{\text{Tr} e^{-\beta\mathcal{H}}}, \quad (2)$$

where  $\beta = 1/T$ . Therefore, any variational ansatz for the density matrix  $X$  provides an upper bound of the actual free energy

$$F \equiv F(X_{\min}) \leq F(X), \quad \forall X > 0 \text{ with } \text{Tr} X = 1. \quad (3)$$

It is also known that, for any positive matrix  $Y$ , the entropy of the distribution  $X$  satisfies the inequality<sup>10</sup>

$$S(X) = -\text{Tr}(X \ln X) \geq -\text{Tr}(X \ln Y) - \text{Tr}(X \ln (X Y^{-1})) \equiv S_{\text{var}}(X, Y). \quad (4)$$

It then follows that, for any positive  $Y$  and  $X$  such that  $\text{Tr} X = 1$ ,

$$F \leq \min_{X,Y} \left\{ \text{Tr}(X\mathcal{H}) - T S_{\text{var}}(X, Y) \right\}. \quad (5)$$

Eq. (5) provides a variational principle for the free energy in terms of the distribution  $X$  and the matrix  $Y > 0$ . Let us assume the variational ansatz

$$X = \mathcal{P} \rho_* \mathcal{P}^\dagger, \quad (6)$$

where

$$\rho_* = \frac{e^{-\beta\mathcal{H}_*}}{\text{Tr} e^{-\beta\mathcal{H}_*}}, \quad (7)$$

is the Boltzmann distribution corresponding to a variational non-interacting Hamiltonian  $\mathcal{H}_*$ , and  $\mathcal{P}$  a many-body operator that we can parametrize as

$$\mathcal{P} = \mathcal{U} \sqrt{\mathcal{Q}}, \quad (8)$$

with unitary  $\mathcal{U}$  and  $\mathcal{Q} > 0$ . It follows that the entropy of the distribution  $X$

$$\begin{aligned} S(X) &= -\text{Tr}(X \ln X) \\ &= -\text{Tr}\left(\mathcal{Q}^{1/2} \rho_* \mathcal{Q}^{1/2} \ln (\mathcal{Q}^{1/2} \rho_* \mathcal{Q}^{1/2})\right), \end{aligned} \quad (9)$$

is independent of the unitary operator  $\mathcal{U}$ . By means of Eq. (4), setting  $Y = \mathcal{Q}$ , we obtain

$$\begin{aligned} S_{\text{var}}(X, Y) &= -\text{Tr}\left(\mathcal{Q}^{1/2} \rho_* \mathcal{Q}^{1/2} \ln \mathcal{Q}\right) \\ &\quad - \text{Tr}\left(\mathcal{Q}^{1/2} \rho_* \mathcal{Q}^{1/2} \ln (\mathcal{Q}^{1/2} \rho_* \mathcal{Q}^{-1/2})\right) \\ &= -\text{Tr}\left(\rho_* \mathcal{Q} \ln \mathcal{Q}\right) - \text{Tr}\left(\rho_* \mathcal{Q} \ln (\rho_*)\right). \end{aligned} \quad (10)$$

In conclusion, given the ansatz Eqs. (6)-(8), one can obtain an upper estimate of the actual free energy

$$\begin{aligned} F \leq \min \left\{ \text{Tr}\left(\rho_* \mathcal{P}^\dagger \mathcal{H} \mathcal{P}\right) + T \text{Tr}\left(\rho_* \mathcal{P}^\dagger \mathcal{P} \ln \mathcal{P}^\dagger \mathcal{P}\right) \right. \\ \left. + T \text{Tr}\left(\rho_* \mathcal{P}^\dagger \mathcal{P} \ln \rho_*\right) \right\}, \end{aligned} \quad (11)$$

minimizing with respect to a non-interacting Hamiltonian  $\mathcal{H}_*$  and a many-body operator  $\mathcal{P}$ . This minimization is feasible only for particular choices of  $\mathcal{P}$ . For instance, if  $\mathcal{P} = 1$ , Eq. (11) reduces to the well-known Hartree-Fock variational estimate of the free energy. Another possibility is that  $\mathcal{P}$  is a two-body Jastrow factor, which can be handled by the variational Monte Carlo statistical approach.<sup>11</sup> In the next section, we shall consider still another class of operators  $\mathcal{P}$ , which can be dealt with analytically in the limit of infinite coordination lattices.

We conclude by noting that, since Eq. (11) is based on the lower bound estimate  $S_{\text{var}}(X, Y)$  of the entropy of the distribution  $X$ , Eq. (10), there is no guarantee that, within a particular class of  $Y$ , such estimate is positive at any temperature, as the true entropy should be. Therefore, it is more appropriate to state that

$$S(X) \geq \max_{Y>0} \left\{ S_{\text{var}}(X, Y), 0 \right\}. \quad (12)$$

We further mention that Eq. (4) is actually the  $p = 1$  case of the more general inequality<sup>10</sup>

$$\begin{aligned} S(X) &= -\text{Tr}(X \ln X) \geq -\text{Tr}(X \ln Y) \\ &\quad - \frac{1}{p} \text{Tr}\left(X \ln (X^p Y^{-p})\right), \end{aligned} \quad (13)$$

which becomes an equivalence as  $p \rightarrow 0$ . We cannot exclude that exploiting Eq. (13) one could get a better but still manageable estimate of the entropy, though we did not succeed.

## III. THE GUTZWILLER APPROXIMATION AT FINITE $T$

We assume a Hamiltonian

$$\mathcal{H} = \sum_{i,j} \sum_{ab} (t_{ij}^{ab} c_{ia}^\dagger c_{jb} + H.c.) + \sum_i \mathcal{H}_i, \quad (14)$$

defined on a lattice with coordination number  $z$ , and hopping parameters  $t_{ij}^{ab}$  such that their contribution to the

total energy is well behaved also in the limit  $z \rightarrow \infty$ .  $\mathcal{H}_i$  includes on-site potential and interaction terms, while  $c_{ia}^\dagger$  creates an electron at site  $i$  with quantum number  $a$ , which can include spin and orbital. Given a variational density matrix of the form as in Eqs. (6) and (7), i.e.

$$\rho_G = \mathcal{P} \rho_* \mathcal{P}^\dagger, \quad (15)$$

we take the operator  $\mathcal{P}$  to be of the Gutzwiller type,<sup>12,13</sup> i.e.

$$\mathcal{P} = \prod_i \mathcal{P}_i, \quad (16)$$

where  $\mathcal{P}_i$  acts on the Hilbert space at site  $i$ . We shall impose that

$$\text{Tr}(\rho_* \mathcal{P}_i^\dagger \mathcal{P}_i) = 1, \quad (17)$$

$$\text{Tr}(\rho_* \mathcal{P}_i^\dagger \mathcal{P}_i \mathcal{C}_i) = \text{Tr}(\rho_* \mathcal{C}_i), \quad (18)$$

where  $\mathcal{C}_i$  is any single-particle operator at site  $i$ . The above conditions replace those at zero temperature<sup>14–16</sup> and allow to analytically compute averages over the distribution function  $\rho_G$  in the limit of infinite coordination number,  $z \rightarrow \infty$  (the proof is exactly the same as in Ref. 16, hence we shall not repeat it here). Specifically, when  $z \rightarrow \infty$ , the two conditions (17) and (18) imply that the distribution  $\rho_G$  has unit trace, and that all the formulas of Ref. 16 hold with the only difference that, instead of averaging over a variational Slater determinant, one has to average over the variational non-interacting Boltzmann distribution  $\rho_*$ . Following Ref. 16, we assume that  $\rho_*$  identifies a local natural basis, with creation operators  $d_{i\alpha}^\dagger$ , related by a unitary transformation to the original operators  $c_{ia}^\dagger$ , such that

$$\text{Tr}(\rho_* d_{i\alpha}^\dagger d_{i\beta}) = \delta_{\alpha\beta} n_{i\alpha}^0, \quad (19)$$

where  $n_{i\alpha}^0$  depends on the variational Hamiltonian  $\mathcal{H}_*$  and on the temperature. We also introduce local Fock states in the natural representation

$$|i; \{n\}\rangle = \prod_\alpha (d_{i\alpha}^\dagger)^{n_\alpha} |0\rangle, \quad (20)$$

whose local probability distribution is diagonal,

$$\begin{aligned} \text{Tr}(\rho_* |i; \{n\}\rangle \langle i; \{m\}|) &= \delta_{\{n\}\{m\}} P_{i;\{n\}}^0 \\ &= \delta_{\{n\}\{m\}} \prod_\alpha (n_{i\alpha}^0)^{n_\alpha} (1 - n_{i\alpha}^0)^{1-n_\alpha}. \end{aligned}$$

We then parametrize the operator  $\mathcal{P}_i$  as

$$\mathcal{P}_i = \sum_{\{n\}, \Gamma} \Phi_{i;\Gamma\{n\}} (P_{i;\{n\}}^0)^{-1/2} |i; \Gamma\rangle \langle i; \{n\}|, \quad (21)$$

where  $\Phi_{i;\Gamma\{n\}}$  are the components of a temperature-dependent variational matrix  $\Phi_i$ , and  $|i; \Gamma\rangle$  are local

basis states in the original representation. In terms of  $\Phi_i$  the Eqs. (17) and (18) read

$$\text{Tr}(\Phi_i^\dagger \Phi_i) = 1, \quad (22)$$

$$\text{Tr}(\Phi_i^\dagger \Phi_i d_{i\alpha}^\dagger d_{i\alpha}) = n_{i\alpha}^0, \quad (23)$$

all other bilinear operators in (23) having null average. If we discard for simplicity the possibility of superconductivity, it follows that<sup>16</sup>

$$\begin{aligned} \text{Tr}(\rho_G \mathcal{H}) &= \sum_{i,j} \sum_{\alpha\beta} \text{Tr}(\rho_* (t_{*ij}^{\alpha\beta} d_{i\alpha}^\dagger d_{j\beta} + H.c.)) \\ &\quad + \sum_i \text{Tr}(\Phi_i^\dagger \mathcal{H}_i \Phi_i), \end{aligned} \quad (24)$$

where

$$t_{*ij}^{\alpha\beta} = \sum_{ab} R_{i\alpha a}^\dagger t_{ij}^{ab} R_{j b \beta}, \quad (25)$$

with the renormalization factors

$$R_{i\alpha a}^\dagger = (n_{i\alpha}^0 (1 - n_{i\alpha}^0))^{-1/2} \text{Tr}(\Phi_i^\dagger c_{ia}^\dagger \Phi_i d_{i\alpha}). \quad (26)$$

In other words, the average over  $\rho_G$  of the Hamiltonian (14) is equal to the average over the uncorrelated distribution  $\rho_*$  of a renormalized hopping Hamiltonian plus the sum of local terms that depend only on the variational matrices  $\Phi_i$ .

We next need to evaluate the entropy. We note that, in the  $z \rightarrow \infty$  limit, and for any, even non-local, single-particle operator  $\mathcal{C}$

$$\text{Tr}(\rho_* \mathcal{P}^\dagger \mathcal{P} \mathcal{C}) = \text{Tr}(\rho_* \mathcal{C}).$$

Since it also holds that

$$\begin{aligned} \text{Tr}(\rho_* \mathcal{P}^\dagger \mathcal{P} \ln \mathcal{P}^\dagger \mathcal{P}) &= \sum_i \text{Tr}(\rho_* \mathcal{P}_i^\dagger \mathcal{P}_i \ln \mathcal{P}_i^\dagger \mathcal{P}_i) \\ &= \sum_i \text{Tr} \left[ \Phi_i^\dagger \Phi_i \ln \left( (P_i^0)^{-1} \Phi_i^\dagger \Phi_i \right) \right], \end{aligned}$$

it follows that Eq. (10) reads, in the  $z \rightarrow \infty$  limit,

$$\begin{aligned} S_{\text{var}}(\rho_*, \Phi^\dagger \Phi) &= S(\rho_*) \\ &\quad - \sum_i \text{Tr} \left[ \Phi_i^\dagger \Phi_i \ln \left( (P_i^0)^{-1} \Phi_i^\dagger \Phi_i \right) \right] \\ &= S(\rho_*) + \sum_i S(\Phi_i^\dagger \Phi_i || P_i^0), \end{aligned} \quad (27)$$

where  $S(\Phi_i^\dagger \Phi_i || P_i^0)$  is the relative entropy between the distribution  $\Phi_i^\dagger \Phi_i$  and the uncorrelated local distribution  $P_i^0$ . In conclusion, the free energy can be upper estimated through

$$F \leq \min \left\{ \sum_{i,j} \sum_{\alpha\beta} \text{Tr}(\rho_* (t_{*ij}^{\alpha\beta} d_{i\alpha}^\dagger d_{j\beta} + H.c.)) \right\}$$

$$+ \sum_i \text{Tr} \left( \Phi_i^\dagger \mathcal{H}_i \Phi_i \right) - T \text{Max} \left( S_{\text{var}}(\rho_*, \Phi^\dagger \Phi), 0 \right) \Big\}, \quad (28)$$

hence one just needs to minimize the r.h.s. supplemented by the constraints (22) and (23). A possible route is to regard  $n_{i\alpha}^0$  in Eqs. (19) and (23) as independent minimization parameters, and introduce two Lagrange multipliers terms

$$\text{Tr}(\rho_* \mathcal{V}) - \sum_i \sum_{\alpha\beta} \mu_{i\alpha\beta} \left[ \text{Tr}(\Phi_i^\dagger \Phi_i d_{i\alpha}^\dagger d_{i\beta}) - \delta_{\alpha\beta} n_{i\alpha}^0 \right],$$

where the non-interacting potential  $\mathcal{V}$  enforces Eq. (19), while  $\mu_{i\alpha\beta}$  enforce Eq. (23).

When  $S_{\text{var}}(\rho_*, \Phi^\dagger \Phi) > 0$ , the saddle point with respect to the uncorrelated distribution  $\rho_*$ , see Eq. (7), corresponds to identifying

$$\mathcal{H}_* = \sum_{i,j} \sum_{\alpha\beta} (t_{*ij}^{\alpha\beta} d_{i\alpha}^\dagger d_{j\beta} + H.c.) + \mathcal{V}, \quad (29)$$

so that, once  $\mathcal{V}$  is chosen so as to satisfy Eq. (19), Eq. (28) reads

$$\begin{aligned} F &\leq \min \left\{ F_*[\Phi, n^0] \right. \\ &+ \sum_i \text{Tr}(\Phi_i^\dagger \mathcal{H}_i \Phi_i) + S(\Phi_i^\dagger \Phi_i || P_i^0) \\ &- \sum_i \sum_{\alpha\beta} \mu_{i\alpha\beta} \left[ \text{Tr}(\Phi_i^\dagger \Phi_i d_{i\alpha}^\dagger d_{i\beta}) - \delta_{\alpha\beta} n_{i\alpha}^0 \right] \Big\} \\ &\equiv \min_{\Phi, n^0, \mu} \left\{ F[\Phi, n^0, \mu] \right\}, \end{aligned} \quad (30)$$

where  $F_*$  is the free energy of non-interacting electrons described by the Hamiltonian  $\mathcal{H}_*$  in (29) that depends on the variational matrices  $\Phi_i$  and on the parameters  $n_{i\alpha}^0$  through the constraint (19) and the Eqs. (25) and (26).

However, when  $T \rightarrow 0$ ,  $S_{\text{var}}(\rho_*, \Phi^\dagger \Phi)$  becomes very small and it may happen that the saddle point of Eq. (28) is only a relative minimum, while the actual minimum is obtained by  $\rho_*$  being the projection onto the ground state of the Hamiltonian  $\mathcal{H}_*$  in Eq. (29). In this case, as well as when  $S_{\text{var}}(\rho_*, \Phi^\dagger \Phi) \leq 0$ , the variational estimate of the free energy coincides with that of the ground state energy, evidently a drawback of the entropy bound that we use. In our experience, this problem may arise only at very low temperature, in which case, although the free energy estimate is continuous, its derivative may not be so. This is evidently not a signal of a genuine first order transition but only a flaw of the method. However, since the temperature when this occurs is extremely low, the entropy contribution is nonetheless negligible, so is the error in the free energy.

Minimization of  $F[\Phi, n^0, \mu]$  therefore provides an upper bound to the actual free energy in lattices with infinite coordination number  $z \rightarrow \infty$ . Seemingly to what it is done at zero temperature, one can keep using the same free-energy functional also when the coordination number is finite, which can be regarded as the finite temperature extension of the Gutzwiller approximation.<sup>12–14</sup> We mention that, in the simple case of a one-band Hubbard model, the free energy functional  $F[\Phi, n^0, \mu]$  coincides with the expression derived by different arguments in Ref. 9.

In the next section we apply the outlined method to a simple two-band Hubbard model and test its results with exact ones obtained by DMFT.

#### IV. A TOY-MODEL FOR $\text{V}_2\text{O}_3$

The model we are going to analyze is inspired by the physics of  $\text{V}_2\text{O}_3$ . In this compound, the  $\text{V}^{2+}$  ions have two valence electrons occupying the conduction bands that originate mainly from the  $t_{2g}$  atomic  $d$ -orbitals. At high temperatures,  $\text{V}_2\text{O}_3$  is a paramagnetic metal but, upon substituting V with Cr it can turn into a paramagnetic insulator.<sup>17</sup> The transition is first order and ends into a second-order critical point. At low temperature,  $\text{V}_2\text{O}_3$  is instead an antiferromagnetic insulator. The Néel transition occurs at  $T_N \simeq 170$  K and is accompanied by a martensitic transformation from the high-temperature corundum structure to the low-temperature monoclinic one.<sup>18</sup> As a result, the magnetic ordering is not a simple G-type, as it could well be in a bipartite lattice, but, in the honeycomb-lattice basal plane, two bonds are antiferromagnetic and one is ferromagnetic.<sup>19</sup> There is wide consensus that the magnetic moment is formed by a spin  $S = 1$ <sup>20</sup> but it is also contributed by angular momentum,<sup>21</sup> signaling a non-negligible spin-orbit coupling. Even though a reliable description of the antiferromagnetic transition requires including electron-lattice and spin-orbit couplings, the main features of the phase diagram can be likely explained ignoring those additional complications. The trigonal field of the corundum structure splits the  $t_{2g}$  orbitals into a lower  $e_g^\pi$  doublet and a higher  $a_{1g}$  singlet. It is therefore tempting to conclude that the low-temperature insulator describes the two electrons in the  $e_g^\pi$  doublet that, because of Hund's rules, are coupled into a spin-triplet. This conclusion is probably not far from reality. Indeed, although the bare value of the crystal field splitting is too small in comparison with the bare conduction bandwidth,<sup>22</sup> strong enough electronic correlations may reverse the situation and stabilize the insulating phase.<sup>23</sup> This scenario has been actually advocated to explain the phase diagram of  $\text{V}_2\text{O}_3$  on the basis of a DMFT-LDA calculation in Ref. 24, and seems supported by some experimental evidences.<sup>25</sup> Indeed, DMFT-LDA results have shown that the effective crystal field splitting  $\Delta_{\text{eff}}$  between  $e_g^\pi$  and  $a_{1g}$  orbitals is enhanced by correlations from its bare value  $\Delta \simeq 0.27$  eV

to one four times larger, which increases as the strength of the electron repulsion.<sup>24</sup> In addition,  $\Delta_{\text{eff}}$  has been found to increase upon lowering temperature  $T$ , though only slightly,<sup>24</sup> but, more importantly, it has been observed that the magnetic susceptibility of the  $e_g^\pi$  increases substantially with lowering  $T$ , while that of the  $a_{1g}$  stays constants<sup>24</sup> or even diminishes,<sup>26</sup> precursor signals of a magnetic instability that involves only  $e_g^\pi$  orbitals.

However, all calculations so far have not been pushed down to the Néel transition temperature to really uncover the proposed mechanism of a gradual depopulation of the  $a_{1g}$ -derived band and concomitant magnetic polarization of the  $e_g^\pi$ -derived ones. Here, we would like to address this issue by exploiting the finite temperature technique described in section II on a simplified model that we believe captures the essential physics. Instead of considering three  $t_{2g}$  orbitals split into two plus one and occupied on average by two electrons, we shall consider only two split orbitals occupied on average by one electron (quarter filling). In this way we miss the important role of Coulomb exchange, which forces the two electrons on the  $e_g^\pi$  doublet to lock into a spin triplet state and might bring about relevant incoherence effects,<sup>27</sup> but the gross features of the phase diagram, in particular the interplay between temperature, crystal field splitting, correlations and magnetism, should be maintained.

Specifically, we shall study the two-band Hamiltonian on a square lattice

$$\mathcal{H} = \sum_{a=1}^2 \sum_{\mathbf{k}\sigma} \epsilon_{\mathbf{k}} c_{a\mathbf{k}\sigma}^\dagger c_{a\mathbf{k}\sigma} + \sum_{\mathbf{k}\sigma} \gamma_{\mathbf{k}} (c_{1\mathbf{k}\sigma}^\dagger c_{2\mathbf{k}\sigma} + H.c.) + \sum_i \left[ -\Delta (n_{1i} - n_{2i}) + \frac{U}{2} (n_{1i} + n_{2i})^2 \right], \quad (31)$$

where  $a = 1, 2$  labels the two orbitals,  $\epsilon_{\mathbf{k}} = -2t(\cos k_x + \cos k_y)$  is the standard nearest neighbor tight-binding energy,  $U$  parametrizes the on-site repulsion and  $\Delta > 0$  the crystal field splitting. We include an inter-orbital hopping  $\gamma_{\mathbf{k}} = -4t' \sin k_x \sin k_y$  with a symmetry such that the local single-particle density matrix remains diagonal in the orbital indices 1 and 2, thus mimicking the  $a_{1g}$ - $e_g^\pi$  hybridization in the corundum phase of  $\text{V}_2\text{O}_3$ .<sup>24</sup> We shall further assume a density corresponding to one electron per site.

In spite of its simplicity, the model in Eq. (31) reproduces qualitatively the actual behavior of  $\text{V}_2\text{O}_3$ . If  $\Delta \simeq t' \ll t$ , which we shall consider hereafter, the model describes a two-band metal for small  $U$ . However, for very large  $U$ , we do expect a Mott insulating phase with the electrons localized mostly on the lowest orbital and antiferromagnetically ordered. Therefore a strong repulsion  $U$  can turn the two band metal into a single-band antiferromagnetic insulator, the two-band analogue of what is predicted in  $\text{V}_2\text{O}_3$ . The question we would like to address here is the behavior at finite temperature.

We first observe that the enhancement of the effective

crystal field  $\Delta_{\text{eff}}$  caused by  $U$ , which eventually leads to antiferromagnetism once the highest band is emptied, can be described also within Hartree-Fock. Indeed, if we neglect magnetism and assume the variational mean-field ansatz

$$\langle n_{1i} \rangle = \frac{1}{2} + \delta n, \quad \langle n_{2i} \rangle = \frac{1}{2} - \delta n,$$

then the Hartree-Fock energies of the orbitals are  $\epsilon_1 = -\Delta + U(3 - 2\delta n)/2$ , and  $\epsilon_2 = \Delta + U(3 + 2\delta n)/2$ , so that the effective crystal-field splitting is, within mean-field,  $\Delta_{\text{eff}} = \Delta + U\delta n > \Delta$ . As  $U$  increases,  $\Delta_{\text{eff}}$  grows hence the highest band depopulates until it becomes completely empty. Beyond this point, only the lowest band remains occupied, specifically half-filled, which can lead to a Stoner-like antiferromagnetic instability, hence to an insulating state. In other words, as we mentioned in the Introduction, an independent particle picture, like Hartree-Fock, is indeed able to explain the occurrence of an antiferromagnetic insulating state at low temperature. However, no matter how large  $U$  is, Hartree-Fock will predict this insulating phase to turn metallic above the Néel temperature  $T_N$ . On the contrary, we expect that, for  $T > T_N$  but  $U$  large enough, the phase should still be insulating, though paramagnetic.

#### A. Finite- $T$ Gutzwiller approximation at work

We can improve the Hartree-Fock description at finite temperature by the Gutzwiller variational approach of section II. By our choice, even though the inter-orbital hybridization  $t'$  is finite, hence the two orbital can mutually exchange electrons, still the local density matrix is diagonal by symmetry. In other words, the natural basis, see Eq. (19), coincides with the original one; a great simplification in the calculations. Since we will search for simple two-sublattice Néel order, we can set, for any site  $i$  belonging to sublattice  $A$ ,  $\Phi_i = \Phi_A \equiv \Phi$  and  $n_{ia\sigma}^0 = n_{Aa\sigma}^0 \equiv n_{a\sigma}^0$  (see Eq. (19)), such that  $\sum_{a\sigma} n_{a\sigma}^0 = 1$ . The variational matrix  $\Phi$  is defined in the local Fock space and is only invariant under spin-rotations around the magnetization axis, which we choose as the  $z$  axis. It follows that, for any site  $i$  belonging to the other sublattice  $B$ ,  $\Phi_i = \Phi_B = U^\dagger \Phi U$  with  $U = \exp(i\pi S_y/2)$  and  $S_y$  the  $y$ -component of the total local spin, while  $n_{ia\sigma}^0 = n_{Ba\sigma}^0 \equiv n_{a-\sigma}^0$ . Because of Eq. (23), we must impose the constraint

$$\text{Tr}(\rho_* c_{ia\sigma}^\dagger c_{ib\sigma'}) = \text{Tr}(\Phi^\dagger \Phi c_{a\sigma}^\dagger c_{b\sigma'}) = \delta_{ab} \delta_{\sigma\sigma'} n_{a\sigma}^0, \quad (32)$$

for  $i \in A$ , while, for  $i \in B$ ,  $\Phi \rightarrow U^\dagger \Phi U$  and  $n_{a\sigma}^0 \rightarrow n_{a-\sigma}^0$ .

Since natural and original bases coincide, the renormalization factors of Eq. (26) are diagonal and read, for  $i \in A$ ,

$$R_{ia\sigma}^* = R_{a\sigma}^* = \frac{1}{\sqrt{n_{a\sigma}^0 (1 - n_{a\sigma}^0)}} \text{Tr}(\Phi^\dagger c_{a\sigma}^\dagger \Phi c_{a\sigma}), \quad (33)$$



while, for  $i \in B$ ,  $R_{i a \sigma}^* = R_{a - \sigma}^*$ . We find that, at the optimized values of the variational parameters,  $R_{i a \sigma}$  are always real. Therefore, if we define  $R_{a \sigma} \equiv R_a + \sigma S_a \in \Re$ , then the variational uncorrelated Hamiltonian  $\mathcal{H}_*$ , see Eq. (7), is

$$\begin{aligned} \mathcal{H}_*[\Phi, n^0] = & \sum_{a=1}^2 \sum_{\mathbf{k}\sigma} \epsilon_{\mathbf{k}a} c_{a\mathbf{k}\sigma}^\dagger c_{a\mathbf{k}\sigma} \\ & + \sum_{\mathbf{k}\sigma} \gamma_{\mathbf{k}}' (c_{1\mathbf{k}\sigma}^\dagger c_{2\mathbf{k}\sigma} + H.c.) \\ & + \sum_{\mathbf{k}\sigma} \sigma \gamma_{\mathbf{k}}'' (c_{1\mathbf{k}\sigma}^\dagger c_{2\mathbf{k}+\mathbf{Q}\sigma} + H.c.) \\ & + \mu \sum_{a\mathbf{k}\sigma} n_{a\mathbf{k}\sigma} + \mu_{\text{CF}} \sum_{\mathbf{k}\sigma} (n_{1\mathbf{k}\sigma} - n_{2\mathbf{k}\sigma}) \\ & + \sum_{a=1}^2 \sum_{\mathbf{k}\sigma} \sigma h_a (c_{a\mathbf{k}\sigma}^\dagger c_{a\mathbf{k}+\mathbf{Q}\sigma} + H.c.), \end{aligned} \quad (34)$$

where  $\mathbf{Q} = (\pi, \pi)$ , the Lagrange multipliers  $\mu$ ,  $\mu_{\text{CF}}$ ,  $h_1$  and  $h_2$  enforce the constraints (32), and

$$\begin{aligned} \epsilon_{a\mathbf{k}} &= (R_a^2 - S_a^2) \epsilon_{\mathbf{k}}, \\ \gamma_{\mathbf{k}}' &= (R_1 R_2 + S_1 S_2) \gamma_{\mathbf{k}}, \\ \gamma_{\mathbf{k}}'' &= (R_1 S_2 + R_2 S_1) \gamma_{\mathbf{k}}. \end{aligned}$$

It follows that, if

$$F_*[\Phi, n^0] = -\frac{T}{N} \ln \text{Tr} \left( e^{-\beta \mathcal{H}_*} \right), \quad (35)$$

where  $N$  is the number of sites, then we have to minimize

$$\begin{aligned} F[\lambda, \Phi, n^0] = & F_*[\Phi, n^0] + \frac{U}{2} \text{Tr} \left( \Phi^\dagger (n_1 + n_2)^2 \Phi \right) \\ & - \Delta \text{Tr} \left( \Phi^\dagger (n_1 - n_2) \Phi \right) \\ & - \sum_{a\sigma} \lambda_{a\sigma} \left[ \text{Tr} \left( \Phi^\dagger \Phi n_{a\sigma} \right) - n_{a\sigma}^0 \right] \\ & - T S(\Phi^\dagger \Phi || P^0), \end{aligned} \quad (36)$$

with the constraint  $\sum_{a\sigma} n_{a\sigma}^0 = 1$ .

We find more convenient to minimize the variational free energy (36) first with respect to all parameters except  $n^0$ ,<sup>8</sup> thus obtaining the functional

$$F[n^0] = \min_{\lambda, \Phi} F[\lambda, \Phi, n^0]. \quad (37)$$

We calculate  $F[n^0]$  in a two-step cyclic process; first we fix  $\Phi$  and minimize  $F_*[\Phi, n^0]$  with respect to the Lagrange multipliers in Eq. (34). Then, at fixed matrix elements  $\langle c_{i a \sigma}^\dagger c_{j b \sigma'} \rangle_{\rho^*}$ , we minimize  $F[\lambda, \Phi, n^0]$  with respect to  $\Phi$  fulfilling the Gutzwiller constraints. This second non-linear constrained minimization is performed by the LANCELOT B routine of the GALAHAD library.<sup>28</sup> This two-step cycle is repeated until convergence. Finally a full minimization of  $F[n^0]$  with respect to  $n^0$  is performed.

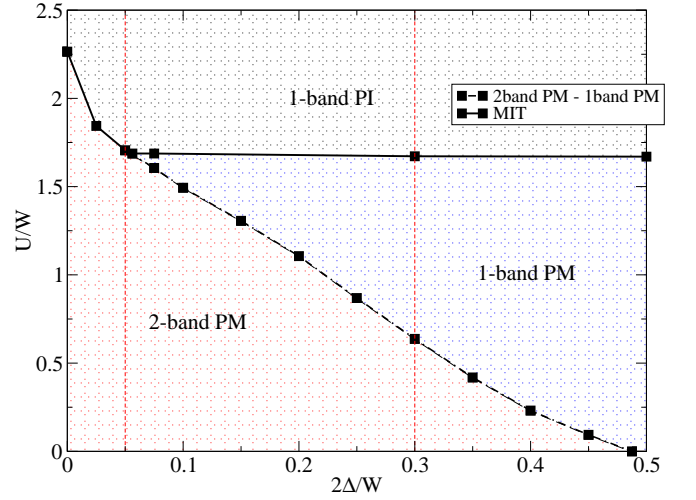


FIG. 1: (Color online)  $T = 0$  phase diagram for model in Eq. (31). The solid line indicates the MIT transition; the dashed/dotted line separates the two-band paramagnetic metal (2-band PM) from the one-band metal (1-band PM). The vertical dashed red lines indicate the values of  $\Delta$  which are used in Fig.2.

## B. $T = 0$ phase diagram

The results that follow are obtained setting  $t = 1/8$  and the inter-orbital hybridization  $t' = 0.3t$ . The  $t' = 0$  bandwidth  $W = 8t = 1$  hence sets the unit of energy.

First we consider the  $T = 0$  case of Eq. (36), which corresponds to the usual Gutzwiller variational approach. In Fig.1 we plot the zero temperature phase diagram in the paramagnetic sector as a function of  $U$  and  $\Delta$ . Our results compare well with the DMFT phase diagram of Refs. 23 and 29. In the limit  $\Delta = 0$  the model undergoes a second order metal-to-insulator transition (MIT) at a critical value  $U_c^{\Delta=0} \simeq 2.27W$ . In the opposite non interacting case,  $U = 0$ , upon increasing  $\Delta$  the system crosses a Lifshitz transition from a two-band to a one-band metal. We note that the majority ( $>$ ) and minority ( $<$ ) bands do not have a unique orbital character, therefore the band polarization  $n_+ - n_-$ , which saturates to 1 at the two-band  $\rightarrow$  one-band transition, is in general different from the orbital polarization  $n_1 - n_2$ .

As anticipated, at finite  $U$  a smaller crystal field splitting is required to induce the two-band  $\rightarrow$  one-band transition, see Fig.1. Above this transition, the ground state is a one-band metal which eventually undergoes a second order MIT at a critical value  $U_c \simeq 1.68W$ . In Fig. 2 (right panel) we show the details of these two subsequent transitions for a value of  $\Delta = 0.3W$ . For  $U \leq 0.64W$ , the two-band metal is stable but, increasing  $U$ , the minority band gradually empties and both renormalization factors,  $R_1$  and  $R_2$ , decrease. At  $U \simeq 0.64W$  the minority band completely depopulates and the left-over half-filled majority band is driven to the MIT at  $U \simeq 1.68W$ . Approaching the MIT, the renormalization

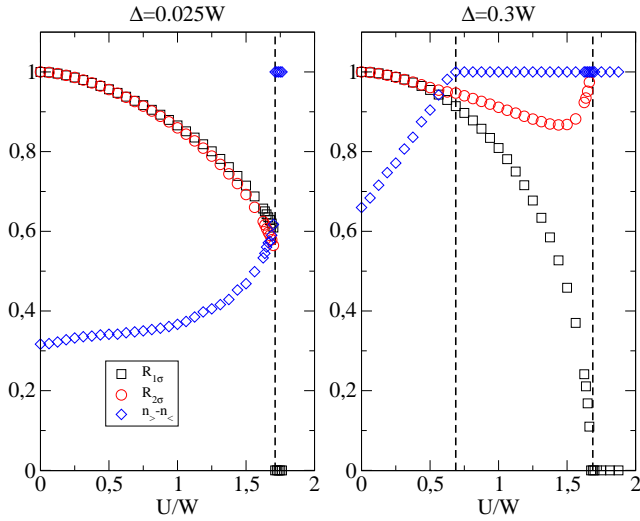


FIG. 2: (Color online)  $n_+ - n_-$  (blue diamonds), renormalization factors  $R_1$  (black squares) and  $R_2$  (red circles) as a function of  $U$  for fixed  $\Delta = 0.025W$  (left panel) and  $\Delta = 0.3W$  (right panel). The vertical dashed lines indicate the two-band  $\rightarrow$  one-band metal transition and the MIT.

factor  $R_1$  of the lowest-energy orbital vanishes, while  $R_2$  actually increases to one – the almost empty orbital undresses from correlations. For smaller  $\Delta$ , the two-band  $\rightarrow$  one-band transition becomes first order and approaches the one-band MIT point, ending in a multicritical point at  $\Delta \simeq 0.028W$ . In Fig.2 (left panel) we plot the behavior of  $R_1$ ,  $R_2$  and  $(n_+ - n_-)$  for  $\Delta = 0.025W$ ; in this case the two renormalization factors are approximately equal and decrease monotonically with  $U$ . At the transition, the majority orbital occupation suddenly increases and the corresponding renormalization factor vanishes. We mention that a Mott insulator with partial occupation of both orbitals can not be stabilized within the Gutzwiller approximation, while more reliable DMFT calculations show that such a phase does exist for very small  $\Delta$ .<sup>29</sup>

If we allow for magnetism, the one-band phases, either metallic or Mott insulating, turn immediately into an antiferromagnetic insulator, see Fig.3. The transition from the two-band paramagnetic metal (2-band PM) to the one-band antiferromagnetic insulator (1-band AFI) is first order and accompanied by a jump in the orbital polarization and in the staggered magnetization, see inset of Fig.3.

### C. $T \neq 0$ phase diagram

We have seen that at zero temperature the ground state is either a one-band antiferromagnetic insulator or a two-band paramagnetic metal. Therefore, as we anticipated, the  $T = 0$  Gutzwiller variational results are not dissimilar from the predictions of the Hartree-Fock approximation. Differences instead arise at finite temperature, where the Gutzwiller variational approach, as

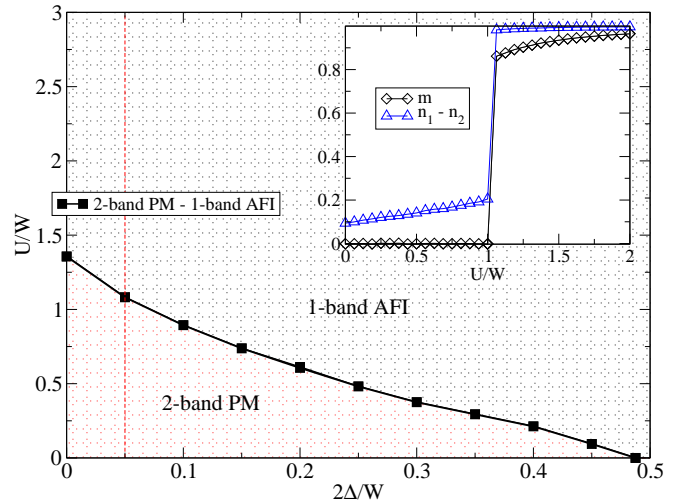


FIG. 3: (Color online) Zero temperature phase diagram allowing for magnetism. The black line separates the two-band paramagnetic metal (2-band PM) from the one-band antiferromagnetic insulator (1-band AFI). In the inset we plot the orbital polarization  $n_1 - n_2$  and the staggered magnetization for a fixed value of  $\Delta = 0.025W$  (red dashed line).

we are going to show, can describe melting of the Néel order without metallization, unlike Hartree-Fock.

We begin as before by restricting the analysis to the paramagnetic sector and consider the case of  $\Delta = 0.025W$ . At zero temperature we found that the model is a 1-band PI for values of  $U \geq 1.7W$ , while a 2-band PM below, Fig.1. At finite temperature, the entropic contribution may favor the paramagnetic insulating solution, like in the single band Hubbard model,<sup>3</sup> thus leading to a finite  $T$  metal-insulator transition. This indeed occurs, as shown in Fig. 4 where we plot the phase diagram as a function of  $U$  and  $T$  (upper panel) and the temperature dependence of the majority orbital  $R_1$  and the orbital polarization (lower panels). In the figure we observe that for values of  $U \geq 1.7W$ , increasing the temperature the orbital polarization decreases and the quasiparticle weight increase: the 1-band PI continuously evolves towards a 2-band PI. Instead, for smaller values of  $U$ , the system is initially a two-band metal and undergoes a first order transition to an insulating state which is accompanied by an abrupt fall-down of the renormalization factors and increase of orbital polarization. As in Ref. 9, we interpret the jump of the renormalization factor as the boundary of the PM-PI transition. Notice that, differently from the  $T = 0$  case, the orbital polarization does not saturate at the transition. Finally, for values of  $U$  smaller than  $\sim 1.19W$ , the quasiparticle weight and the orbital polarization evolve smoothly to the high temperature limit, displaying a dip that we interpret as the crossover regime. We estimate the end-point of the transition at  $T \simeq 0.09W$ .

We note, in the lower panel of Fig. 4 and for  $U = 1.1W$ , the tiny discontinuity of  $R_1$  and  $n_1 - n_2$  at  $T \simeq$

$0.01W$ , which is consequence of the aforementioned artificial discontinuity in the slope of the free energy caused by our not rigorous lower bound of the entropy.

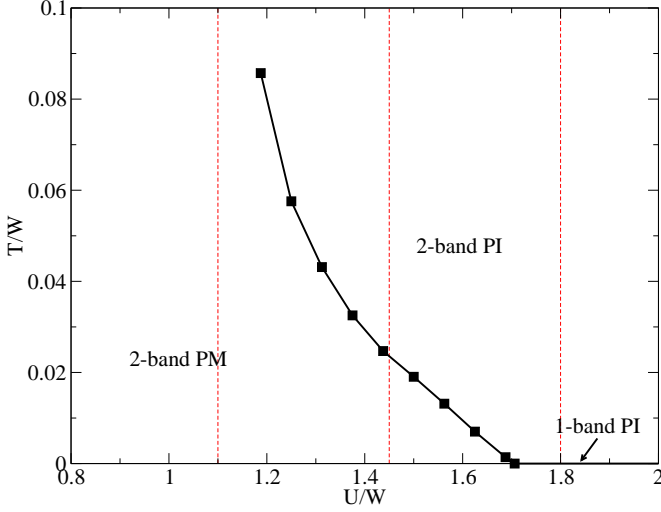


FIG. 4: (Color online) Upper panel: phase diagram in the paramagnetic domain. The black line separates the PM phase from the PI one. The red vertical lines indicate the values of  $U$  plotted in the lower panel.

Lower panel: Temperature dependence of the quasiparticle renormalization factor for the majority orbital (left) and of the orbital polarization (right) for different values of  $U$ .

When magnetism is allowed, at zero temperature and at large  $U$  the ground state is antiferromagnetic. At finite temperature the system remains ordered up to the Néel temperature. In Fig. 5 we plot for  $\Delta = 0.025W$  the phase diagram, indicating by a dotted line the PM-PI transition that we have found in the paramagnetic sector. We note that the PM-PI transition line crosses the Néel temperature, roughly at  $U \simeq 1.28W$ , and extends above. For  $U > 1.28W$ , the Gutzwiller variational approach is able to describe melting of the AFI into a 2-band PI, which we mentioned is not accessible by Hartree-Fock.

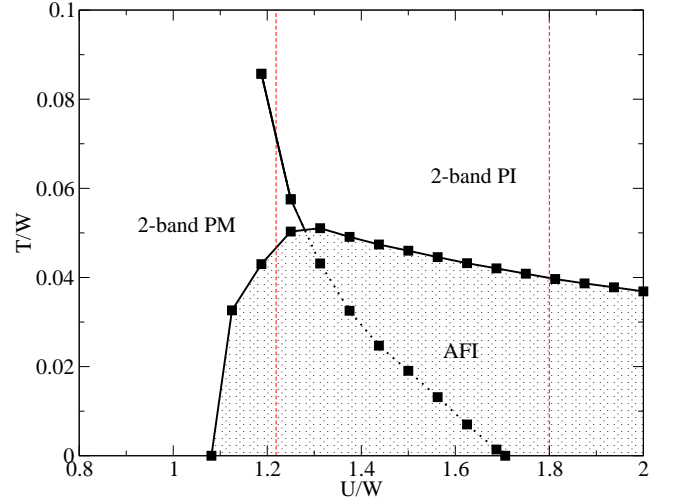


FIG. 5: (Color online) Finite temperature phase diagram as a function of  $U$  and  $T$ , for a fixed value of  $\Delta = 0.025W$ . The paramagnetic solution is continued also within the AFM domain (dotted line). The vertical red dashed line indicates the temperature cut represented in Fig.6.

For smaller values of  $U$ , the magnetic insulator turns into a 2-band PM that eventually undergoes a Mott transition at higher temperatures. In Fig. 6 we show more in detail the behavior of the physical quantities across the different transitions; in the low temperature AFI (blue area on the left) the orbital and magnetic polarizations are very weakly temperature dependent. Increasing  $T$ , the Néel order melts, the orbital polarization decreases (red areas on the right), and the model turns into a 2-band PM (left panel) or PI (right panel) depending on the value of  $U$ . In the former case, left panel of Fig. 6, the 2-band PM is eventually driven to the PI state, transition that is signaled by the sudden vanishing of the renormalization factors and the jump of the orbital polarization  $n_1 - n_2$ . In the right panel, instead, the AFI melts directly in the PI; the renormalization factor vanishes at the transition and then smoothly increases from zero on raising  $T$ .

We observe that the finite temperature phase diagram of Fig. 5 is not dissimilar to that of  $V_2O_3$  as function of chemical/physical pressure. Also the physical mechanism that controls the phase diagram, i.e. the correlation enhanced crystal-field splitting, is consistent with that proposed in Ref. 24 for  $V_2O_3$ , though in our case the number of orbitals involved is two and not three. We also note the discontinuous increase of the orbital polarization across the PM to PI transition upon increasing temperature, see right panel in Fig. 6, which is consistent with X-ray adsorption spectra of  $V_2O_3$ ,<sup>20,30</sup> in which case the orbital polarization relates to the occupation of the  $e_g^\pi$  orbitals with respect to the  $a_{1g}$  one.



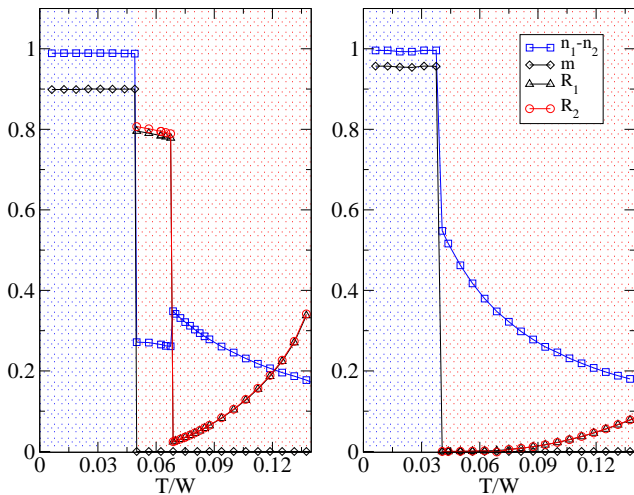


FIG. 6: (Color online) The blue (to the left in each panel) and red areas (to the right) indicate respectively the AFI phase and the paramagnetic phases as a function of temperature at fixed values of  $U = 1.22W$  (left panel) and  $U = 1.8W$  (right panel). At low temperatures the orbital polarization (blue squares) and the staggered magnetization (black squares) are practically equal to the zero temperature values and display a discontinuous jump at the AFI-paramagnetic transition. In the paramagnetic phase we show also the behavior of the renormalization factors whose jump indicates the PM-PI transition.

## V. COMPARISON WITH DMFT

In this section, we compare the quality of the finite temperature Gutzwiller approximation with exact DMFT results. In particular, we shall consider a simplified version of the model in Eq. (31) with vanishing inter-orbital hybridization,  $t' = 0$ , and on a Bethe lattice with only nearest neighbor hopping, which leads to a non-interacting semicircular density of states of bandwidth  $W$ . We choose a Bethe lattice (a Cayley tree with coordination number  $z \rightarrow \infty$ ) because in this case DMFT is exact and, as previously discussed, the Gutzwiller approximation does provide a rigorous upper bound to the free energy, which therefore makes it possible to assess its accuracy with respect to exact results. The phase diagrams obtained by DMFT and by the Gutzwiller approximation in the  $U$ - $T$  space for  $\Delta = 0.025W$  are shown in Fig. 7.

DMFT maps the lattice model onto an impurity model, which, in the present calculation, is solved by means of exact diagonalization<sup>31</sup> in the finite-temperature implementation proposed in Ref. 32, which is particularly accurate at the low temperatures that we consider. Within the exact diagonalization approach, the bath is approximated by a finite number,  $N_b$ , of energy levels. Here we take  $N_b = 10$  and  $N_b = 12$ , i.e. 5 and 6 bath levels for each physical orbital. Only for  $N_b = 10$  we could include a number of states sufficient to obtained converged results. Therefore data for  $N_b = 12$  have only

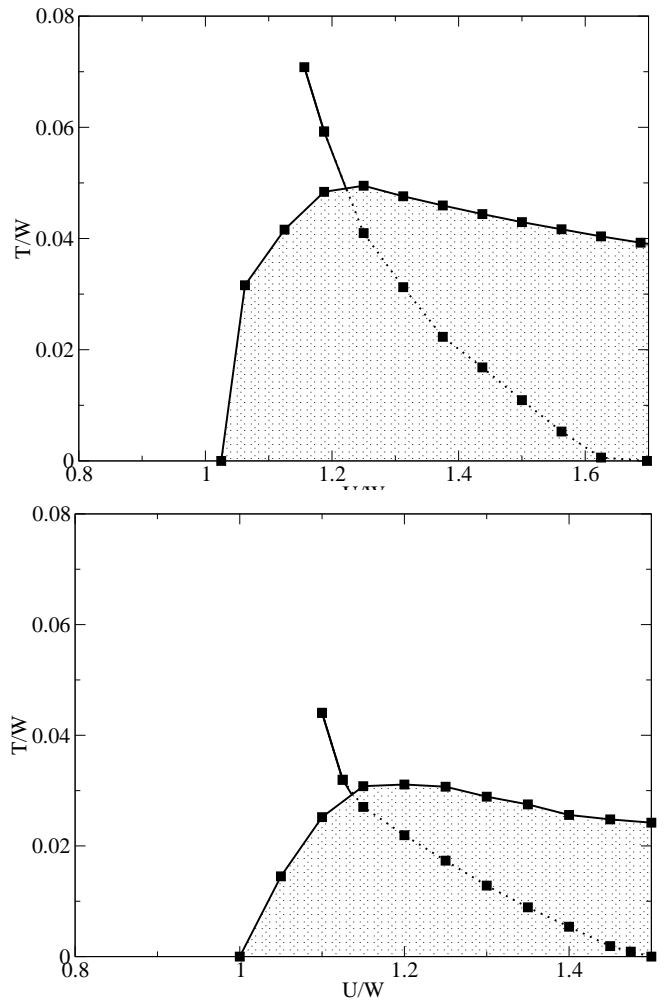


FIG. 7: Top panel: finite  $T$  phase diagram within the Gutzwiller approximation at  $\Delta = 0.025W$ ,  $t' = 0$  and a semicircular DOS. Bottom panel: same as before but within DMFT, which is exact.

obtained for low temperatures, and used to prove that the discretization error only leads to minor corrections to the phase diagram. We consider both paramagnetic and antiferromagnetic solutions. As customary, we first determine the Mott transition line in the paramagnetic sector by comparing the free energies of the metallic and Mott insulating solutions. The transition is first-order at any finite temperature and ends in a finite-temperature critical point at  $T \lesssim 0.05W$ . If we allow for long-range antiferromagnetic order, at  $T = 0$  the system is metallic for  $U \lesssim W$ , and it turns into a single-band antiferromagnet for larger values of the interaction. The Néel temperature rapidly grows with  $U$  and reaches a maximum around  $U \simeq 1.2W$ , above which it monotonically decreases. However, differently from the single-band case, the first-order Mott line is not completely covered by the antiferromagnetic dome.

The DMFT phase diagram is thus very similar to that

obtained by the finite-temperature Gutzwiller approach, qualitatively and to same extent also quantitatively, see Fig. 7. As common with the Gutzwiller approximation, the  $T = 0$  Mott transition in the paramagnetic sector occurs at larger  $U/W \simeq 1.7$  than the exact DMFT value  $U/W \simeq 1.5$ . In addition, the Gutzwiller wavefunction seems to overestimate antiferromagnetism, which occupies a larger region in the phase diagram. However, quite remarkably, the critical endpoints of the PM-PI Mott transition do not differ much,  $U/W \simeq 1.17$  and  $T/W \simeq 0.07$  in the Gutzwiller calculation, while  $U/W \simeq 1.15$  and  $T/W \simeq 0.05$  in DMFT.

## VI. CONCLUSIONS

Using some rigorous trace inequalities, we have derived an upper-bound estimate of the free energy of an interacting-electron Hamiltonian for variational density matrices of Gutzwiller and Jastrow type. We have then exploited this result to extend to finite temperature the conventional Gutzwiller approximation, which in turn becomes an exact variational approach in lattices with infinite coordination number.

We have applied this technique to calculate the finite-temperature phase diagram of a two-band model that we believe captures qualitatively well the physics of vanadium sesquioxide,  $V_2O_3$ .

In spite of being extremely simplified with respect to a complete description of  $V_2O_3$ , the model has a very similar phase diagram comprising a low-temperature antiferromagnetic insulating dome and high-temperature paramagnetic metal as well as Mott insulating phases separated by a first order line with a second-order critical endpoint. We have tested the accuracy of our finite temperature Gutzwiller approximation comparing the phase diagram of the model on a Bethe lattice with the exact one obtained by DMFT. The agreement is qualitatively very satisfying and partly also quantitatively. We believe therefore that this simple variational technique is very promising to attach correlated electron systems at finite temperature, and could be used whenever more reliable tools, like DMFT, become numerically too demanding.

## Acknowledgments

We thank Nicola Lanatà and Giovanni Borghi for very useful discussions and helpful suggestions. This work has been supported by the European Union, Seventh Framework Programme, under the project GO FAST, Grant Agreement no. 280555 and the European Research Council Starting Grant SUPERBAD, Grant Agreement no. 240524.

- 
- <sup>1</sup> V. Eyert, Phys. Rev. Lett. **107**, 016401 (2011), URL <http://link.aps.org/doi/10.1103/PhysRevLett.107.016401>
  - <sup>2</sup> G. Sangiovanni, A. Toschi, E. Koch, K. Held, M. Capone, C. Castellani, O. Gunnarsson, S.-K. Mo, J. W. Allen, H.-D. Kim, et al., Phys. Rev. B **73**, 205121 (2006), URL <http://link.aps.org/doi/10.1103/PhysRevB.73.205121>.
  - <sup>3</sup> A. Georges, G. Kotliar, W. Krauth, and M. J. Rozenberg, Rev. Mod. Phys. **68**, 13 (1996).
  - <sup>4</sup> G. Kotliar, S. Y. Savrasov, K. Haule, V. S. Oudovenko, O. Parcollet, and C. A. Marianetti, Rev. Mod. Phys. **78**, 865 (2006), URL <http://link.aps.org/doi/10.1103/RevModPhys.78.865>.
  - <sup>5</sup> S. Biermann, F. Aryasetiawan, and A. Georges, Phys. Rev. Lett. **90**, 086402 (2003), URL <http://link.aps.org/doi/10.1103/PhysRevLett.90.086402>.
  - <sup>6</sup> X. Y. Deng, L. Wang, X. Dai, and Z. Fang, Phys. Rev. B **79**, 075114 (2009), URL <http://link.aps.org/doi/10.1103/PhysRevB.79.075114>.
  - <sup>7</sup> G. Borghi, Ph.D. thesis, International School for Advanced Studies (SISSA) (2011), URL <http://hdl.handle.net/1963/5358>.
  - <sup>8</sup> N. Lanatà, H. U. R. Strand, X. Dai, and B. Hellsing, Phys. Rev. B **85**, 035133 (2012), URL <http://link.aps.org/doi/10.1103/PhysRevB.85.035133>.
  - <sup>9</sup> W.-S. Wang, X.-M. He, D. Wang, Q.-H. Wang, Z. D. Wang, and F. C. Zhang, Phys. Rev. B **82**, 125105 (2010), URL <http://link.aps.org/doi/10.1103/PhysRevB.82.125105>.
  - <sup>10</sup> D. Petz, in *Functional analysis and operator theory* (Banach Center Publications, 1994), pp. 287–298, URL <http://www.renyi.hu/~petz/pdf/64.pdf>.
  - <sup>11</sup> S. Sorella, Phys. Rev. B **71**, 241103 (2005).
  - <sup>12</sup> M. C. Gutzwiller, Phys. Rev. **134**, A923 (1964).
  - <sup>13</sup> M. C. Gutzwiller, Phys. Rev. **137**, A1726 (1965).
  - <sup>14</sup> J. Bünemann, W. Weber, and F. Gebhard, Phys. Rev. B **57**, 6896 (1998).
  - <sup>15</sup> M. Fabrizio, Phys. Rev. B **76**, 165110 (2007).
  - <sup>16</sup> M. Fabrizio, in *New Materials for Thermoelectric Applications: Theory and Experiment*, edited by V. Zlatić and A. Hewson (Springer, 2013), NATO Science for Peace and Security Series - B: Physics and Biophysics, pp. 247–272.
  - <sup>17</sup> D. B. McWhan, A. Menth, J. P. Remeika, W. F. Brinkman, and T. M. Rice, Phys. Rev. B **7**, 1920 (1973), URL <http://link.aps.org/doi/10.1103/PhysRevB.7.1920>.
  - <sup>18</sup> D. B. McWhan and J. P. Remeika, Phys. Rev. B **2**, 3734 (1970), URL <http://link.aps.org/doi/10.1103/PhysRevB.2.3734>.
  - <sup>19</sup> R. M. Moon, Phys. Rev. Lett. **25**, 527 (1970), URL <http://link.aps.org/doi/10.1103/PhysRevLett.25.527>.
  - <sup>20</sup> J.-H. Park, L. H. Tjeng, A. Tanaka, J. W. Allen, C. T. Chen, P. Metcalf, J. M. Honig, F. M. F. de Groot, and G. A. Sawatzky, Phys. Rev. B **61**, 11506 (2000), URL <http://link.aps.org/doi/10.1103/PhysRevB.61.11506>.
  - <sup>21</sup> L. Paolasini, C. Vettier, F. de Bergevin, F. Yakhov, D. Mannix, A. Stunault, W. Neubeck, M. Altarelli, M. Fabrizio, P. A. Metcalf, et al., Phys. Rev. Lett. **82**, 4719 (1999), URL <http://link.aps.org/doi/10.1103/PhysRevLett.82.4719>.
  - <sup>22</sup> L. F. Mattheiss, Journal of Physics: Condensed Matter **6**, 6477 (1994), URL <http://stacks.iop.org/0953-8984/6/i=32/a=009>.

- <sup>23</sup> N. Manini, G. E. Santoro, A. Dal Corso, and E. Tosatti, Phys. Rev. B **66**, 115107 (2002), URL <http://link.aps.org/doi/10.1103/PhysRevB.66.115107>.
- <sup>24</sup> A. I. Poteryaev, J. M. Tomczak, S. Biermann, A. Georges, A. I. Lichtenstein, A. N. Rubtsov, T. Saha-Dasgupta, and O. K. Andersen, Phys. Rev. B **76**, 085127 (2007), URL <http://link.aps.org/doi/10.1103/PhysRevB.76.085127>.
- <sup>25</sup> M. K. Stewart, D. Brownstead, S. Wang, K. G. West, J. G. Ramirez, M. M. Qazilbash, N. B. Perkins, I. K. Schuller, and D. N. Basov, Phys. Rev. B **85**, 205113 (2012), URL <http://link.aps.org/doi/10.1103/PhysRevB.85.205113>.
- <sup>26</sup> D. Grieger, C. Piefke, O. E. Peil, and F. Lechermann, Phys. Rev. B **86**, 155121 (2012), URL <http://link.aps.org/doi/10.1103/PhysRevB.86.155121>.
- <sup>27</sup> L. de' Medici, J. Mravlje, and A. Georges, Phys. Rev. Lett. **107**, 256401 (2011), URL <http://link.aps.org/doi/10.1103/PhysRevLett.107.256401>.
- <sup>28</sup> N. I. M. Gould, D. Orban, and P. L. Toint, ACM Transactions on Mathematical Software **29**, 353 (2003).
- <sup>29</sup> A. I. Poteryaev, M. Ferrero, A. Georges, and O. Parcollet, Phys. Rev. B **78**, 045115 (2008), URL <http://link.aps.org/doi/10.1103/PhysRevB.78.045115>.
- <sup>30</sup> F. Rodolakis, P. Hansmann, J.-P. Rueff, A. Toschi, M. W. Haverkort, G. Sangiovanni, A. Tanaka, T. Saha-Dasgupta, O. K. Andersen, K. Held, et al., Phys. Rev. Lett. **104**, 047401 (2010), URL <http://link.aps.org/doi/10.1103/PhysRevLett.104.047401>.
- <sup>31</sup> M. Caffarel and W. Krauth, Phys. Rev. Lett. **72**, 1545 (1994), URL <http://link.aps.org/doi/10.1103/PhysRevLett.72.1545>.
- <sup>32</sup> M. Capone, L. de' Medici, and A. Georges, Phys. Rev. B **76**, 245116 (2007), URL <http://link.aps.org/doi/10.1103/PhysRevB.76.245116>.